

Investigating the influence of longitudinal tilt angles on the performance of small scale linear Fresnel reflectors for urban applications

A. Barbón ^a, C. Bayón-Cueli ^c, L. Bayón ^{b,*}, L. Rodríguez ^d

^a Department of Electrical Engineering, University of Oviedo, Campus of Gijón, Spain

^b Department of Mathematics, University of Oviedo, Campus of Gijón, Spain

^c Polytechnic School of Engineering of Gijón, University of Oviedo, Spain

^d Integrated Center of F.P. Maintenance and Services to the Production of Langreo, Spain

ARTICLE INFO

Article history:

Received 29 March 2019

Received in revised form

22 May 2019

Accepted 24 May 2019

Available online 30 May 2019

Keywords:

Small-scale linear Fresnel reflector

Longitudinal inclination

Available area

Energy-to-area ratio

ABSTRACT

The potential use of the small scale linear Fresnel reflectors in building applications can help European Union countries meet their sustainable development goals. The sizing of a small scale linear Fresnel reflector directly influences its primary cost as well as the annual energy output and, hence, its financial attractiveness. In addition, the area required for its installation is a critical parameter in most of the urban applications. This paper presents the analysis of the effects of the longitudinal inclination of the rows of mirrors and/or the absorber tube on the performance of small scale linear Fresnel reflectors. The effect of three parameters (i.e. energy absorbed by the absorber tube, energy area ratio, and primary cost) is evaluated for five cities in European Union. Different combinations of longitudinal tilt angles are analyzed and compared with the typical configuration of a large scale linear Fresnel reflector. Numerical simulations were carried out using a MATLAB code to calculate the energy absorbed by the absorber tube, the energy area ratio, and the primary cost. The comparison of the configurations provided insight into how latitude impacts on the results. It will be demonstrated that the energy absorbed by the absorber tube increase strongly with longitudinal tilt angles, and the primary cost increases weakly with longitudinal tilt angles, while the energy-to-area ratio decreases.

© 2019 Elsevier Ltd. All rights reserved.

1. Introduction

Buildings account for nearly 40% of the European Union's final energy consumption and 36% of its CO₂ emissions [1]. International Energy Agency predicts that if no energy efficiency improvements are carried out in the building sector, energy consumption might increase by 50% in 2050 [2].

Promotion of low energy buildings and zero energy buildings are considered as one of energy efficiency policy tools in European Union. The European Commission promotes an overall reduction in the CO₂-emission levels for the building sector of 88%–91%, compared to 1990 levels, by 2050 [3].

The Energy Efficiency Directive [4] includes a requirement for member states to develop long-term renovation strategies for their

national building stocks. One of important aspects is use of solar energy [1]. Solar energy is the main source of the earth's energy. This helps to reduce both energy consumption and greenhouse gas emissions. Solar energy collectors can be used in active solar systems [5]. Active solar systems contain one or various collectors to heat the water, which is then used in domestic water heating, and spaces heating. Solar concentrating collectors are one of the effective alternatives for the building sector. For example, the parabolic trough collectors ([6,7]) and the small scale linear Fresnel reflectors (SSLFRs).

The possibility of using an SSLFR for conversion of solar energy in urban areas has been explored in recent years. For example: in domestic water heating: [8–10]; in the heating/cooling systems of buildings: [11–13]; in the absorption of cooled air Solar-GAX cycle: [14]; in the absorption cooling system [15]; in daylighting systems [16]. Besides, the small scale linear Fresnel reflectors are among the cheapest solar energy concentration technologies [17].

Some of the main differences among large scale linear Fresnel

* Corresponding author.

E-mail address: bayon@uniovi.es (L. Bayón).

reflectors lie on them having a multiple absorber tube or single-absorber tube, the mirrors being curved or flat, the tracking system design, etc [18]. All these designs have in common that the rows of mirrors and the absorber tube are parallel to the horizontal plane. However, the SSLFR has some flexibility in this regard: their design allows the rows of mirrors to individually rise and descend on the horizontal plane [19] and change the longitudinal inclination of the rows of mirrors and/or the absorber tube can be [20–22]. Other designs combine simultaneously these previous works [23].

The location of the absorber tube with respect to the longitudinal centre of the mirror axis and its relation with the longitudinal inclination of the rows of mirrors and/or the absorber tube, has been studied in Ref. [21]. With the length of the absorber tube constant, the variation of the longitudinal position of the absorber tube leads to decreases of up to 80% in the energy produced [22]. This is due to the increase in end loss and reflected light loss [24]. In order to compute the longitudinal position and length of the absorber tube we will use the algorithm proposed in Ref. [21] to determine the optimal values of the longitudinal position and length of the absorber tube. This algorithm allows the optimization of the position and length of the absorber tube based on the longitudinal design. This method is based on a geometrical algorithm that minimizes the area between two curves, thereby minimizing the end loss and reflected light loss, which are now taken into consideration. The optimal values for the longitudinal position and length of the absorber vary for each geographical location [22], and are related directly with the longitudinal tilt angle of the rows of mirrors and the longitudinal tilt angle of the absorber tube.

The installation of SSLFR in urban applications depends on two fundamental aspects: the European standards and the available flat roof area.

- European Union legislation is a major driver in the use of energy from renewable sources in new and renovated buildings. Directive 2009/28/EC [25] implements the promotion of the use of energy from renewable sources. The Commission Communication established a policy framework for climate and energy in the period from 2020 to 2030 [26]. And the Directive 2018/30/EC [27] establishes numerous requirements concerning the use of renewable energy in new and renovated buildings. The required minimum amount of energy is calculated depending on the climate zone.
- For the local energy production, the roofs of buildings are the optimal location. Besides, the total floor area of residential buildings is around 19 billion (m^2) in the EU [28]. Single family houses represent two thirds of the residential floor space. But the building components (such as chimneys, elevator machine rooms, fans and plumbing vents) reduce the available roof area. Several studies have shown this reduction which ranges from 21% [29] to 30% [30]. The available area is one of the main limiting factors of the local energy production in buildings [31] and is, thus, a critical parameter.

In this paper we study the effects of the longitudinal tilt angle of the rows of mirrors and the longitudinal tilt angle of the absorber tube in terms of energy absorbed by the absorber tube, surface required for installation, and the primary cost. These parameters were calculated based on MATLAB codes especially developed for this study. For the sake of comparison, 5 European geographic locations were studied, in order to evaluate the impact of the latitude in the results.

The paper is organized as follows. The components, parameters, and configurations of the SSLFR are described in Section 2. In Section 3, the parameters used in the comparative analysis are presented. Numerical simulations are presented in Section 4 for

different configurations of the SSLFR. Finally, Section 5 summarizes the main contributions and conclusions of the paper.

Nomenclature

A	Reflector area (m^2)	
	Effective area of the absorber tube (m^2)	
	Primary cost of the assembly (€)	
	Primary cost of the foundation (€)	
	Primary cost of the fixed structure (€)	
	Primary cost of the mobile structure (€)	
	Primary cost of the movement system (€)	
	Primary cost of the mirrors system (€)	
	Primary cost of the secondary reflector system (€)	
	Total primary cost (€)	
	Primary cost of the tracking system (€)	
	Cleanliness factor of the glass	
	Cleanliness factor of the mirror	
	D	Diameter of the absorber tube (m)
	Direct Normal Irradiance (W/m^2)	
d	Separation between two consecutive mirrors (m)	
E	Annual total energy (MWh)	
	energy-to-area ratio (MWh/m^2)	
f	Height of the receiver (m)	
	Incidence angle modifier	
L	Reflector length (m)	
	Length of the mirrors (m)	
	Length of the single absorber tube (m)	
	Left length of the single absorber tube (m)	
	Right length of the single absorber tube (m)	
	Total illuminated length of the absorber tube (m)	
	Left illuminated length of the absorber (m)	
	Right illuminated length of the absorber (m)	
	n	Number of mirrors at each side of the central mirror
		Ordinal of the day (day)
W	Mirror field width (m)	
	Width of the mirrors (m)	
	Width illuminated on the absorber by the i -th by mirror (m)	
	Absorptivity of the absorber tube	
	Angle between the absorber tube and the horizontal plane ($^\circ$)	
	Angle between the mirror axis and the horizontal plane ($^\circ$)	
	Optical efficiency (%)	
	Zenith angle of the Sun ($^\circ$)	
	λ	Latitude angle ($^\circ$)
	μ	Angle between the reflected ray and the normal to the NS axis ($^\circ$)
ρ	Reflectivity of the primary mirrors	
τ	Transmissivity of the glass	

2. Considerations of an SSLFR

2.1. Components

A small scale linear Fresnel reflector, as shown in Fig. 1, consists of parallel rows of stretched mirrors (primary reflector system (3)), that track the sun's daily movement along a single axis (transmission system (5) and tracking system (6)), concentrates direct solar beams onto the focal line of an absorber tube (secondary reflector system (4)). The secondary reflector system (see Fig. 2) is composed of: absorber tube (8), receiver cavity (9), insulation (10), and glass covering (11). The absorber tube (8) is encased in the receiver cavity (9) to reduce convective heat losses and specially coated so as to increase the absorption capability of the incident solar radiation. The receiver cavity (9) is sealed with a glass cover (11) and silicon rubber beading. The concentrated solar energy is transferred through the absorber tube (8) into some thermal fluid capable of maintaining liquid state at high temperatures. The secondary reflector system (4) sits at an appropriate height above the primary reflector system (4). The rows of mirrors (7) are mounted on a mobile structure (2) which allows keeping them with a certain

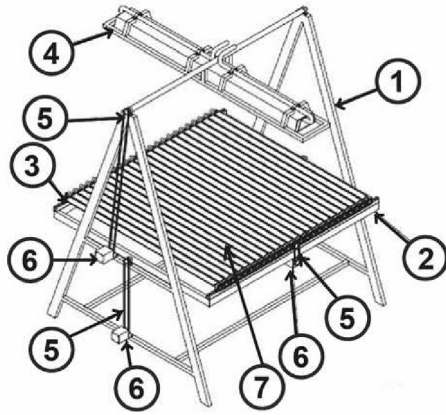


Fig. 1. SSLFR parts.

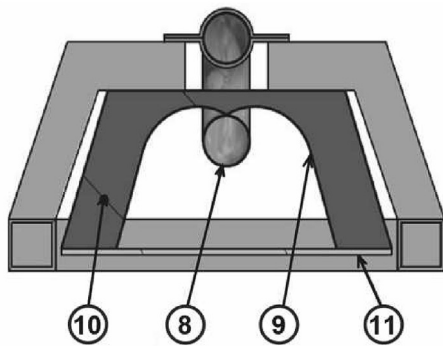


Fig. 2. Secondary reflector system.



Fig. 3. Photograph of an SSLFR prototype.

longitudinal inclination with respect to the horizontal plane. The mobile structure (2) and the secondary reflector system (3) are supported by the fixed structure (1). Fig. 3 shows a photograph of an SSLFR prototype. See Ref. [32] for a more detailed information on a small scale linear Fresnel reflector.

The following assumptions are made in the present study:

- (i) Mobile structure. The mobile structure forms an angle β_M with the horizontal plane. We do not consider possible misalignments.
- (ii) Primary reflector system. The pivoting point of each mirror coincides with the central point of the mirror; hence, it is always focused on the central point of the absorber tube. The mirrors are flat and specularly reflecting and all have the same length and width. Given the uniform distribution of the reflected solar rays (due to the flat geometry of the mirrors), the sun shape does not affect the incoming to the receiver cavity solar irradiance [33].
- (iii) Secondary reflector system. The secondary reflector system forms an angle β_a with the horizontal plane. A single absorber tube is used. We consider that all the solar irradiance that reaches the aperture of the cavity is going to be directed on the absorber tube.
- (iv) Transmission systems: tracking errors and misalignment are not considered.
- (v) Tracking system. The primary reflector systems are perfectly tracked so as to follow the apparent movement of the Sun.
- (vi) We consider that SSLFR is perfectly aligned in a North-South orientation.

- (vii) The area required for the SSLFR installation may not exceed $10 \text{ (m}^2\text{)}$, and derived from this assumption, the values of β_M and β_a are between 0 and certain angle λ .

2.2. Basic parameters

Figs. 4 and 5 show the schematics of a small scale linear Fresnel reflector. To be clearer, some important parameters are presented in these figures. These can be divided into transversal (see Fig. 4) and longitudinal parameters (see Fig. 5) [20]. The transversal ones are: the number of mirrors at each side of the central mirror (n), the mirror width (W_M), the separation between two consecutive mirrors (d), the height of the receiver (f), the diameter of the absorber tube (D), position with respect to the central mirror (L_i), tilt (β_i), and the angle between the vertical at the focal point and the line connecting the centre point of each mirror to the focal point (α_i). The

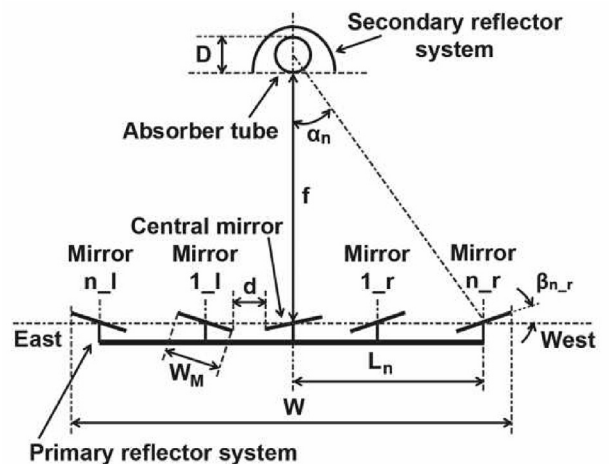


Fig. 4. Schematic front view.

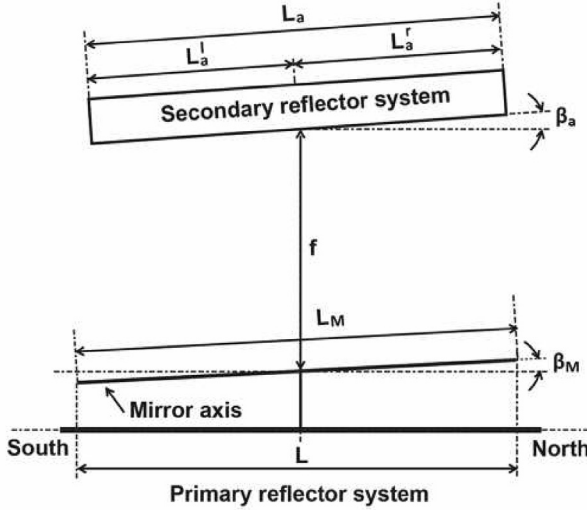


Fig. 5. Schematic side view.

longitudinal parameters are: the mirror length (L_M), the total length of the single absorber tube (L_a), the left length of the single absorber tube (l_a^l), the right length of the single absorber tube (l_a^r), the angle between the mirror axis and the horizontal plane (β_M), and the angle between the absorber tube and the horizontal plane (β_a).

3. Parameters used for the comparison

Obviously, an increase in the length of the absorber tube would increase the absorbed energy, but also the area needed for installation. In some scenarios the available area is a critical parameter. Therefore, we will divide the study into two cases: (i) the available area is not a critical parameter, and (ii) the available area is a critical parameter. The evaluation of each of the configurations is carried out by means of the annual energy absorbed by the absorber tube, if the available area is not a critical parameter. If the available area is a critical parameter the evaluation will include the energy-to-area ratio (EAR). As the economic aspect is very important for the commercialization of these solar concentrators, the primary cost will also be studied. These parameters are defined as follows.

3.1. Energy absorbed by the absorber tube

The total annual energy absorbed by the absorber tube is calculated as:

$$E = \sum_{n_d=1}^{365} \left[\int_0^{24} \left(\sum_{i=0}^{2 \cdot n} DNI^{n_d}(T_S) \cdot \eta_{opt} \cdot IAF_i^{n_d}(T_S) \cdot A_{eff}^{n_d}(T_S) \right) dT_S \right] \quad (1)$$

where: DNI is the direct normal irradiance; η_{opt} is the total optical yield, which is calculated considering the reflectivity of the mirrors (ρ), the cleanliness factors of the mirror (CI_m) and of the glass covering the secondary absorber (CI_g), the transmissivity of this glass (τ), and the absorptivity of the material of which the absorber tube is made (α_b), (see equation (2)); IAF_i measures the variation in the optical performance of an SSLFR for varying ray incidence angles, by the i -th mirror; A_{eff} is the effective area of the absorber tube of the i -th mirror which is actually illuminated; T_S is the solar time; n is the number of mirrors at each side of the central mirror, n_d is the ordinal of the day. η_{opt} can be calculated as:

$$\eta_{opt} = (\rho \cdot CI_m) \cdot (\tau \cdot CI_g \cdot \alpha_b) \quad (2)$$

In equation (1), A_{eff} has a strong dependence on the longitudinal tilt angles, β_M and β_a . A_{eff} can be calculated as:

$$A_{eff} = L_{ai} \cdot l_a; \quad 0 \leq i \leq 2n \quad (3)$$

The term A_{eff} is proportional to the total illuminated length of the absorber tube (l_a) and the length of the circumference illuminated on the absorber tube by the i -th mirror (L_{ai}). The value of l_a is given by:

$$l_a = l_a^l + l_a^r \quad (4)$$

where l_a^l is the left illuminated length of the absorber, and l_a^r is the right illuminated length of the absorber (see Fig. 6). These parameters can be calculated as:

$$l_a^l = \frac{x_0 + \frac{L_M}{2} \cos \beta_M}{\cos \beta_a} \quad (5)$$

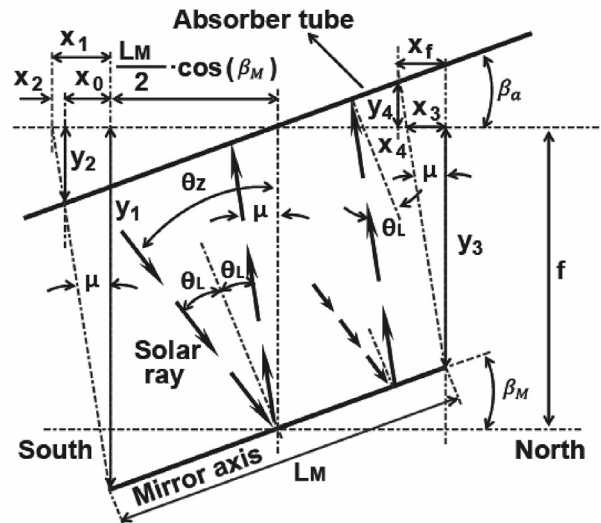
$$l_a^r = \frac{\frac{L_M}{2} \cos \beta_M - x_f}{\cos \beta_a} \quad (6)$$

In the sign convention we have adopted, lengths from the centre of the mirror to the left are considered positive, and those to the right, negative. x_0 and x_f are auxiliary parameters:

$$x_0 = \frac{\left[f + \frac{L_M}{2} [\sin \beta_M - \cos \beta_M \tan \beta_a] \right] \tan(2\beta_M - \theta_z)}{1 + \tan \beta_a \tan(2\beta_M - \theta_z)} \quad (7)$$

$$x_f = \frac{\left[f + \frac{L_M}{2} [\cos \beta_M \tan \beta_a - \sin \beta_M] \right] \tan(2\beta_M - \theta_z)}{1 + \tan \beta_a \tan(2\beta_M - \theta_z)} \quad (8)$$

A deduction of these equations can be consulted in Ref. [21]. The value of L_{ai} is given by (see Fig. 7):

Fig. 6. Deduction of the parameters l_a^l and l_a^r .

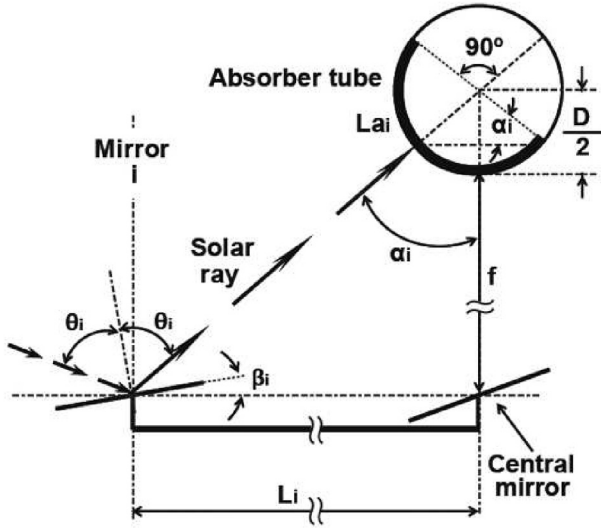


Fig. 7. Deduction of the parameter L_{ai} .

$$L_{ai} = \begin{cases} \frac{\pi D}{2} & \text{if } W_{ai} \cos \alpha_i > D \\ D \arcsin\left(\frac{W_{ai}}{D}\right) & \text{if } W_{ai} \cos \alpha_i \leq D \end{cases} \quad (9)$$

where W_{ai} is the illuminated width on the absorber tube by the i -th mirror is given by:

$$W_{ai} = W_M [\cos \beta_i \pm \sin \beta_i \tan \alpha_i]; \quad 0 \leq i \leq 2n \quad (10)$$

The sign \pm must be adopted according to the following criteria: – for the left side, and + for the right side. A deduction of these equations can be consulted in Ref. [20].

3.2. Energy-to-area ratio

The energy-to-area ratio (*EAR*), which is expressed in MWh/m^2 /year, is commonly used to compare *SSLFR* for urban applications [34]. The *EAR* is obtained by dividing the annual total energy absorbed by the absorber tube in Megawatt hours by area required for the *SSLFR* installation in square meters. The *EAR* is expressed as follows:

$$EAR = \frac{E}{A} \quad (11)$$

The reflector area can be calculated as:

$$A = W \cdot L \quad (12)$$

where W is the mirror field width, and L is the reflector length. The mirror field width can be calculated as (see Fig. 4):

$$W = 2 \cdot n \cdot (W_M + d) + W_M \quad (13)$$

And the reflector length can be calculated with the following relations (see Fig. 5):

$$L = \begin{cases} L_M \cos(\beta_M) & \text{if } \begin{cases} L_a^l \cos(\beta_a) \leq \frac{1}{2} L_M \cos(\beta_M) \\ L_a^r \cos(\beta_a) \leq \frac{1}{2} L_M \cos(\beta_M) \end{cases} \\ L_a^l \cos(\beta_a) + \frac{1}{2} L_M \cos(\beta_M) & \text{if } \begin{cases} L_a^l \cos(\beta_a) > \frac{1}{2} L_M \cos(\beta_M) \\ L_a^r \cos(\beta_a) \leq \frac{1}{2} L_M \cos(\beta_M) \end{cases} \\ \frac{1}{2} L_M \cos(\beta_M) + L_a^r \cos(\beta_a) & \text{if } \begin{cases} L_a^l \cos(\beta_a) \leq \frac{1}{2} L_M \cos(\beta_M) \\ L_a^r \cos(\beta_a) > \frac{1}{2} L_M \cos(\beta_M) \end{cases} \end{cases} \quad (14)$$

The optimal choice of values L_a^l and L_a^r has already been studied in detail in Ref. [21]; they dependence strongly on the longitudinal tilt angles, β_M and β_a .

3.3. Primary cost

The authors [32] developed a detailed *SSLFR* cost model including the primary cost of each *SSLFR* component and subsystem. The total primary cost C_T of an *SSLFR* is given by the sum of the individual costs of the eight components:

$$C_T = C_{FS} + C_{MS} + C_{MOS} + C_{MIS} + C_{SRS} + C_{TS} + C_A + C_F \quad (15)$$

where C_{FS} is the primary cost of the fixed structure (€), C_{MS} is the primary cost of the mobile structure (€), C_{MOS} is the primary cost of the mirrors system (€), C_{MIS} is the primary cost of the movement system (€), C_{SRS} is the primary cost of the secondary reflector system (€), C_{TS} is the primary cost of the tracking system (€), C_A is the primary cost of the assembly works (€), and C_F is the primary cost of the foundation (€). The primary cost equation for each element and its relation with the parameters of an *SSLFR* can be consulted in Ref. [32].

4. Results and discussion

The aim of this section is to estimate the effect of the angle between the mobile structure and the horizontal plane (β_M), and the angle between the secondary reflector system and the horizontal plane (β_a) on various parameters like the annual energy absorbed by the absorber tube, the energy-to-area ratio, and the primary cost. These parameters are analyzed for several geographic locations, and compared with the configuration C_1 , used in large-scale *LFRs*, where the mobile structure and the secondary reflector system form an angle of 0° with the horizontal plane.

The climate where the building is located will affect the local energy production. Besides, according to the European Union legislation commented upon in the Introduction, it is interesting to make this study in different countries of the European Union. The conclusions can be extrapolated to other countries. In the report [43] (See Table 16.) the European countries are grouped in 5 European climate zones based on global radiation, heating degree-days, cooling degree-days and cooling potential by night ventilation. The cities are selected according to several election criteria:

each city must belong to a different climate area and the latitude has to be different enough to allow a meaningful analysis. In this study, five cities are considered. Table 1 shows the geographic characteristics of the cities under study.

In order to carry out this work, specific software has been developed in MATLAB code. The developed code incorporates modules which use a discretization of 10 min to calculate: direct normal irradiance, variation in the optical performance, longitudinal position, effective area of the absorber tube by the *i*-th mirror that is actually illuminated. The shading, blocking, end loss effects, and end reflected light loss were also taken into account. A derived database and system integrating data (PVGIS) [35] were used to estimate the solar irradiance.

The parameters of the SSLFR listed in Table 2, remain constant in this study.

Table 3 shows the parameters: L_a , L_a^l , and L_a^r , for the C_1 configuration, in Almeria, Rome, Budapest, Berlin, and Helsinki, respectively. These values have been calculated using the algorithm proposed in Ref. [21].

With the sign convention that we have adopted, lengths from the centre of the mirror to the left are considered positive, and those to the right, negative.

All the comparisons are being done based on the configuration C_1 , typical for large-scale linear Fresnel reflectors.

4.1. Effects on the annual energy absorbed by the absorber tube

Table 4 shows the annual energy absorbed by the absorber tube in Almeria, Rome, Budapest, Berlin, and Helsinki, respectively. As expected, the maximum annual energy absorbed by the absorber tube happens in Almeria, where the direct normal irradiance is largest.

Figs. 8–12 show the percentages, with respect to configuration C_1 , of the annual energy absorbed by the absorber tube in Almeria, Rome, Budapest, Berlin and Helsinki, respectively.

When the secondary reflector system is at an angle of $\beta_a = 0^\circ$ with respect to the horizontal plane, and the mobile structure is at a specific angle with respect to the same horizontal plane, an increase in β_M decreases the energy absorbed by the absorber tube down to a minimum value and then increases it up to $\beta_M = \lambda$.

The idea is based upon equations (4)–(8) for the particular case of $\beta_a = 0^\circ$. In equation (1) *E*, the total annual energy absorbed by the absorber tube is proportional to $A_{eff}^{n_d}(T_S)$, and this area is directly proportional to $l_a = l_a^l + l_a^r$, which is the sum of the left and right illuminated length of the absorber. So, if we consider $\beta_a = 0^\circ$ in equations (5) and (6) and substitute x_0 and x_f with the values obtained from equations (7) and (8), we get:

$$l_a = l_a^l + l_a^r = L_M \sin(\beta_M) \tan(2\beta_M - \theta_z) + L_M \cos(\beta_M) \quad (16)$$

The zenith angle of the sun (θ_z), is usually written as the complementary of the height angle of the sun ($\theta_z = \frac{\pi}{2} - \alpha_S$). Bearing in mind that the maximum value of the height angle of the sun (α_S) is $\alpha_{S \max} = \frac{\pi}{2} - (\lambda - \delta)$, we have that the minimum value of the zenith angle of the sun at solar noon is $\theta_{zmin} = \frac{\pi}{2} - \alpha_{S \max} = \lambda$. So, if we

Table 1
Cities under study.

Zone	Cities	Latitude	Longitude	Altitude
Zone 1	Almeria (Spain)	36°50'07"N	02°24'08"W	22 (m)
Zone 2	Rome (Italy)	41°53'30"N	12°30'40"E	52 (m)
Zone 3	Budapest (Hungary)	47°29'52"N	19°02'23"E	111 (m)
Zone 4	Berlin (Germany)	52°31'27"N	13°24'37"E	37 (m)
Zone 5	Helsinki (Finland)	60°10'10"N	24°56'07"E	26 (m)

Table 2
Parameters constants used in the study.

Parameters	Value
Number of mirrors at each side of the central mirror	12 [21,22]
Mirror width	0.06(m) [21,22,36]
Separation between two consecutive mirrors	0.024 (m) [20–22]
Diameter of the absorber tube	0.0486 (m) [21,22]
Height of the receiver	1.5 (m) [21,22,36,37]
Mirror length	2.0 (m) [20,22]
Concentration ratio	9.83 [20,22]
Aperture width of the cavity	0.186 (m) [22]
Reflectivity of the mirrors	0.94 [40]
Cleanliness factors of the mirror	0.96 [41]
Cleanliness factors of the glass covering the secondary absorber	0.96 [41]
Transmissivity of this glass	$\tau = 0.87$ if $\alpha_i \leq 20^\circ$, $\tau = 0.85$ if $20^\circ \leq \alpha_i \leq 30^\circ$ [42]

Table 3
Optimization of the length and position of the absorber tube.

	Configuration C_1		
	L_a^l	L_a^r	L_a
Almeria	−0.037	−2037	2.00
Rome	−0.329	−2.329	2.00
Budapest	−0.586	−2.586	2.00
Berlin	−0.865	−2.865	2.00
Helsinki	−1.343	−3.343	2.00

Table 4
Annual energy absorbed by the absorber tube (MWh).

Configuration	Almeria	Rome	Budapest	Berlin	Helsinki
C_1	6.37	4.25	2.40	2.23	1.50

represent l_a (16) as function of β_M , for $\beta_M \in [0, \lambda]$ we get a function with a minimum.

The minimum value is reached at different angles β_M , depending on the localization of the SSLFR. These minimum values are 80.39%, 85.17%, 89.32%, 93.69%, 93.03%, at Almeria, Rome, Budapest, Berlin and Helsinki, respectively. That is, the inclination of just the mobile structure produces first a decrease and then an increase of the annual absorbed energy by the absorber tube.

Table 5 shows the maximum annual energy absorbed by the absorber tube in Almeria, Rome, Budapest, Berlin, and Helsinki, respectively. These results show positive effects of the longitudinal inclination of the mobile structure and the secondary reflector system on the annual energy absorbed by the absorber tube. They show also the effect of latitude on the results.

As we said previously, when the secondary reflector system forms an angle $\beta_a = 0^\circ$ with respect to the horizontal plane, the energy absorbed by the absorber tube is represented by a curve which presents a minimum value. This is true for all locations (latitudes).

However, when the angle β_a is not zero, the situation is different. We see in the locations with the higher latitude (Budapest, Berlin and Helsinki), that when β_a is greater than 50% of λ , the energy reaches a maximum instead of a minimum. This maximum is obtained for different values of β_M . In places with less latitude, such as Almeria or Rome, the effect is not so noticeable.

4.2. Effects on the EAR

Table 6 shows the EAR, for C_1 configuration, in Almeria, Rome,

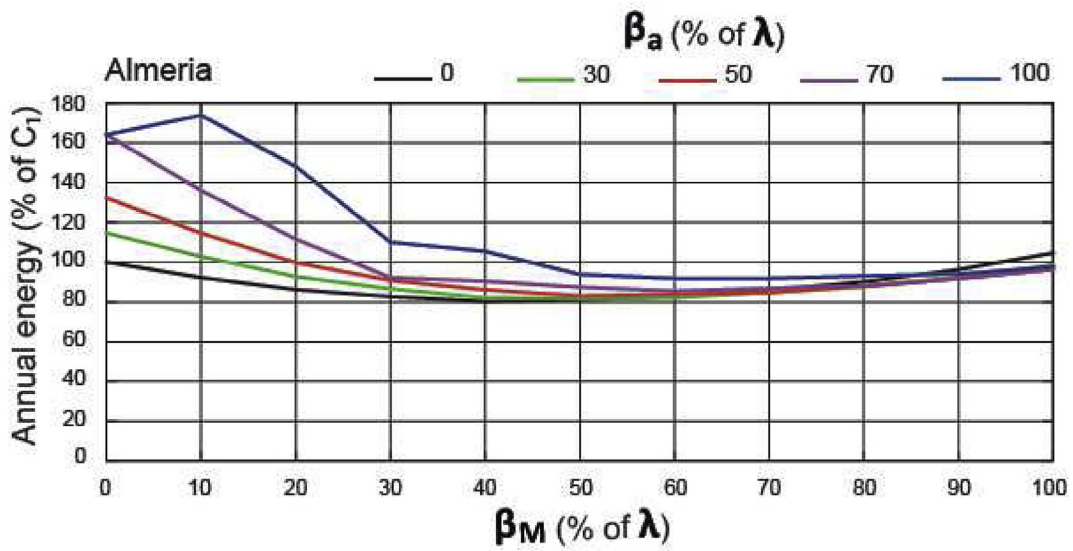


Fig. 8. Comparison annual absorbed energy, in Almeria.

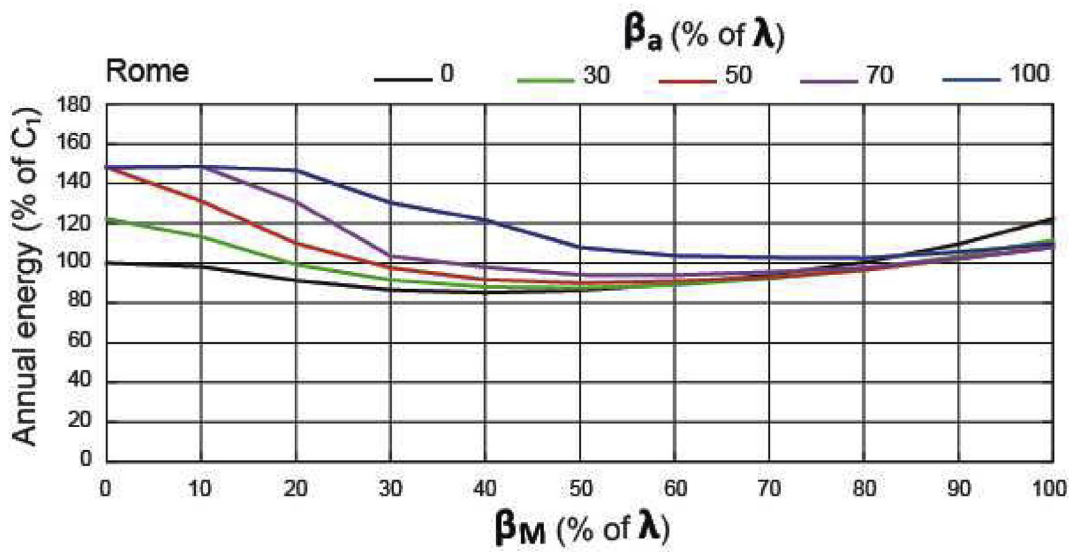


Fig. 9. Comparison annual absorbed energy, in Rome.

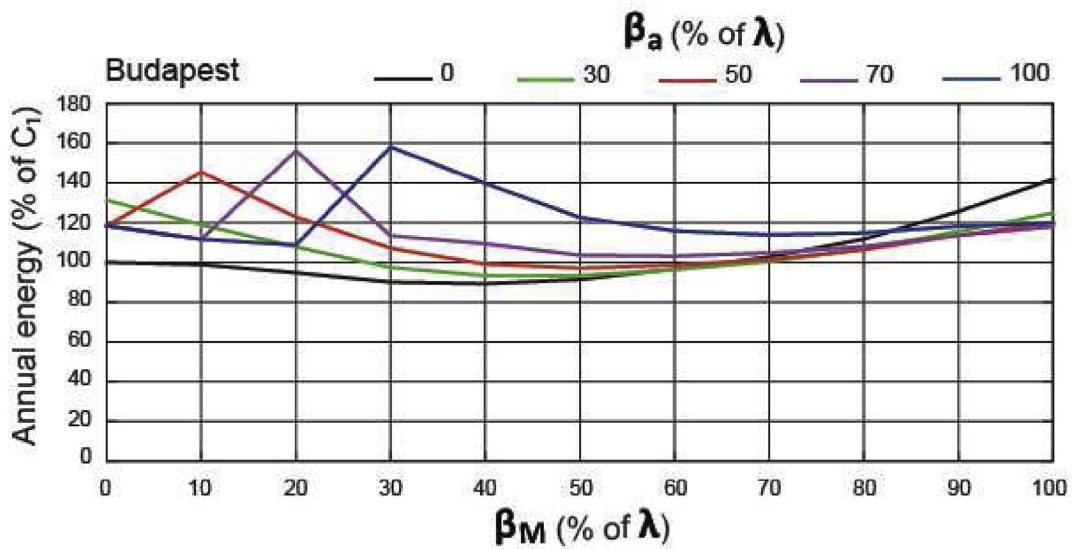


Fig. 10. Comparison annual absorbed energy, in Budapest.

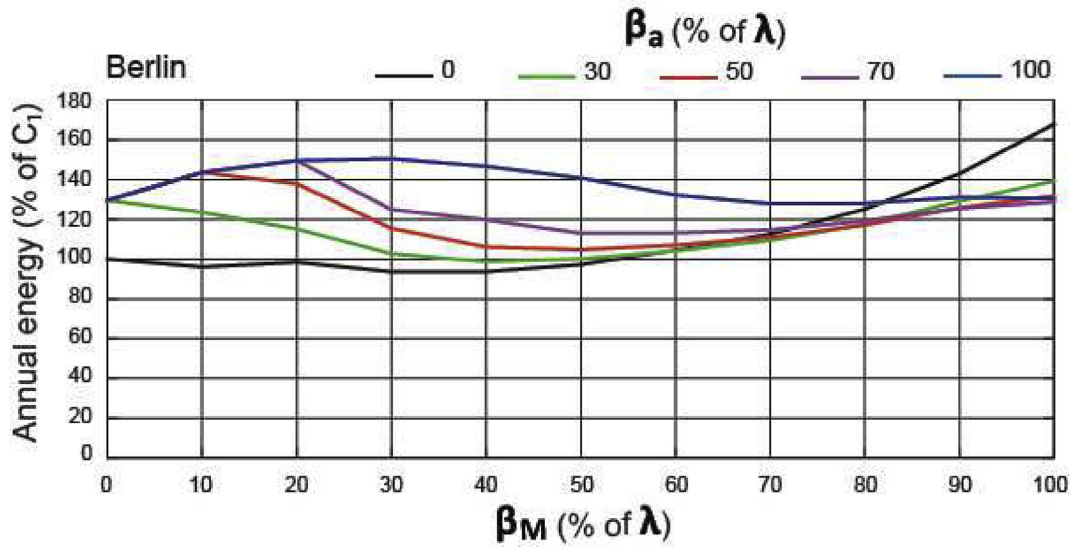


Fig. 11. Comparison annual absorbed energy, in Berlin.

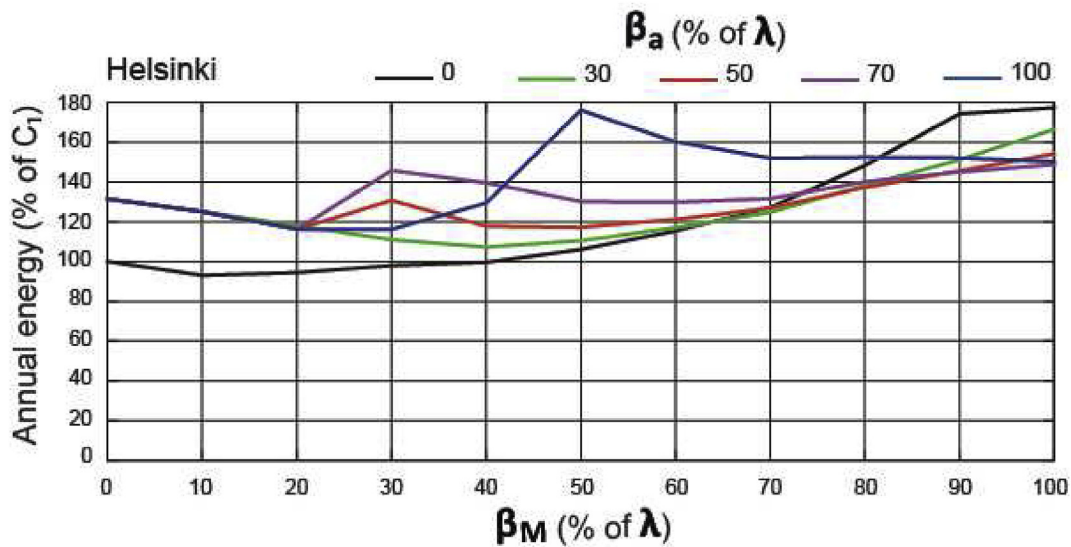


Fig. 12. Comparison annual absorbed energy, in Helsinki.

Table 5
Maximum annual energy absorbed by the absorber tube.

	β_M (% of λ)	β_a (% of λ)	E (% of C_1)
Almeria	10	90	173.95
Rome	10	70	148.55
Budapest	20	70	156.11
Berlin	100	0	167.93
Helsinki	100	0	177.35

Table 6
EAR(MWh/m²).

Configuration	Almeria	Rome	Budapest	Berlin	Helsinki
C_1	1.01	0.64	0.32	0.28	0.15

Table 7
EAR_{maximum} (MWh/m²).

Configuration	Almeria	Rome	Budapest	Berlin	Helsinki
$\beta_M = \frac{\lambda}{2}; \beta_a = \lambda$	1.44	1.15	0.71	0.76	0.63

Budapest, Berlin, and Helsinki, respectively. As expected, the greatest EAR happens in Almeria, where the direct normal irradiance is largest.

The maximum EAR values are obtained for $\beta_M = 50\%$ of λ , $\beta_a = 100\%$ of λ , at all geographic locations. Table 7 shows the EAR, for $\beta_{M\ opt}$ and $\beta_{a\ opt}$, in the cities under study.

The maximum value of EAR is obtained at Almeria because it is the location with the most direct horizontal irradiance. Compared

to Helsinki, it receives more than quadruple the direct horizontal irradiance. However, the value of EAR is not quadruple due to the effect of latitude: the greater the latitude the longer the absorber tube without an increase of the surface needed for installation of

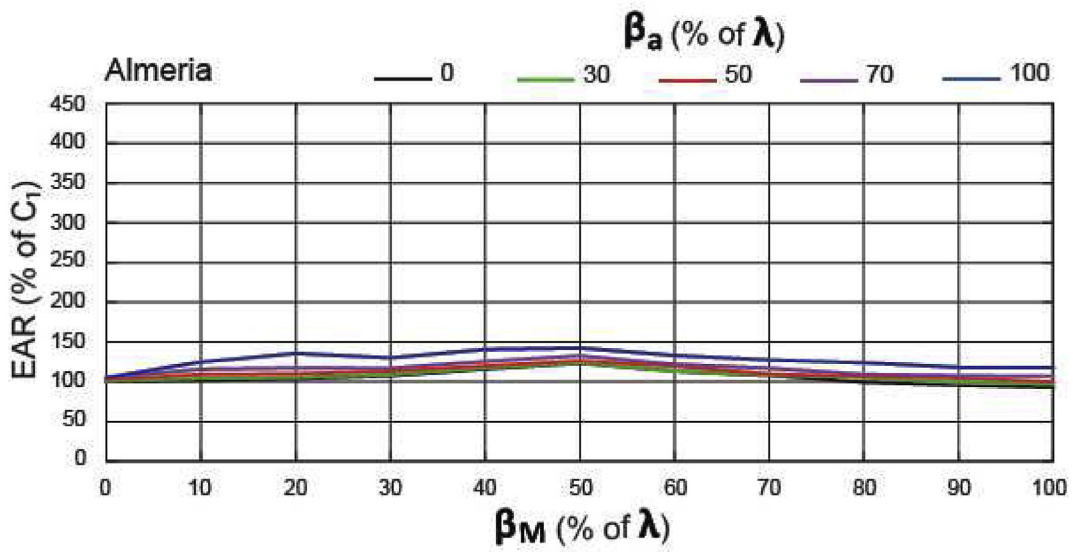


Fig. 13. Comparison EAR, in Almeria.

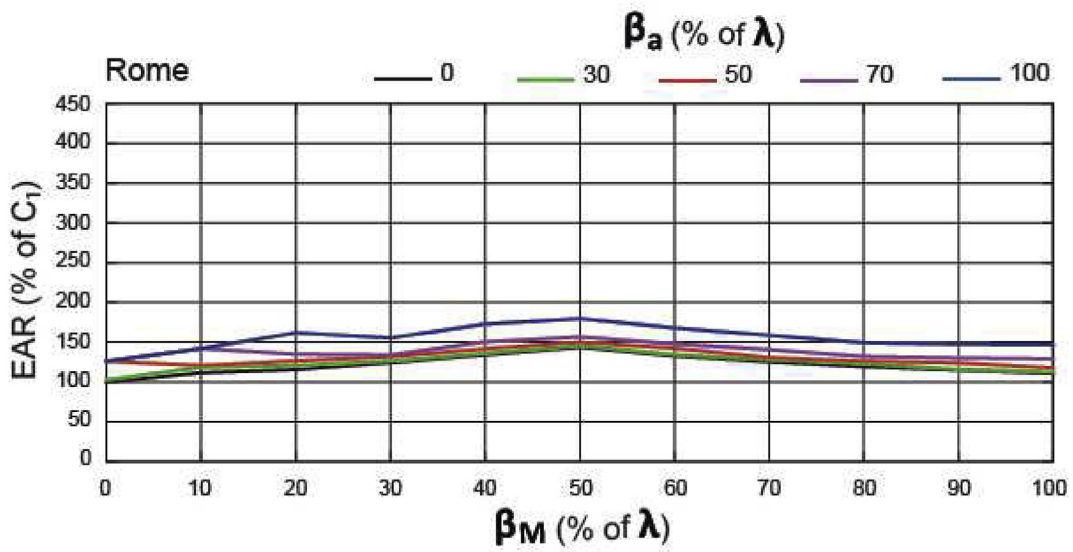


Fig. 14. Comparison EAR, in Rome.

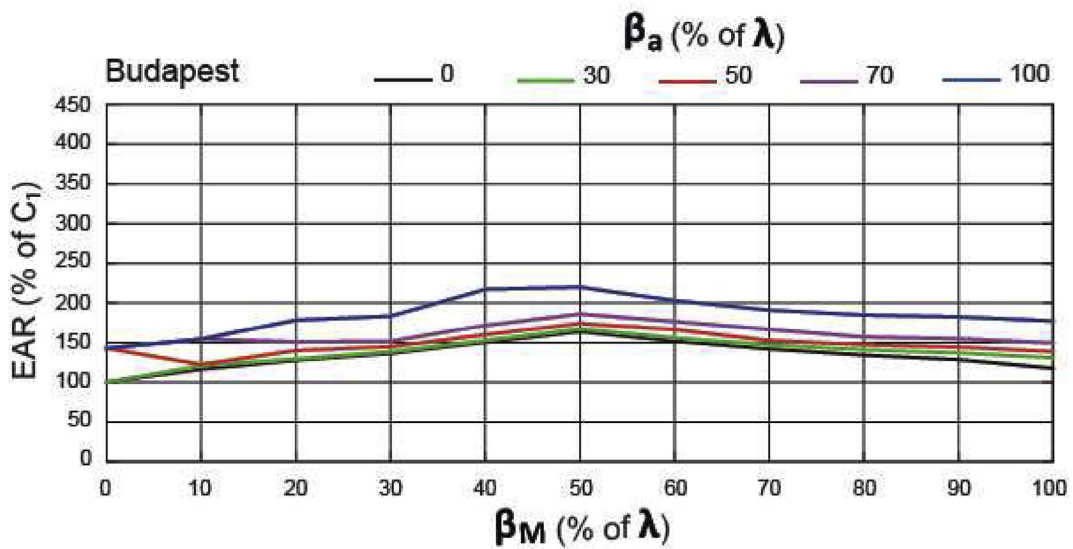


Fig. 15. Comparison EAR, in Budapest.

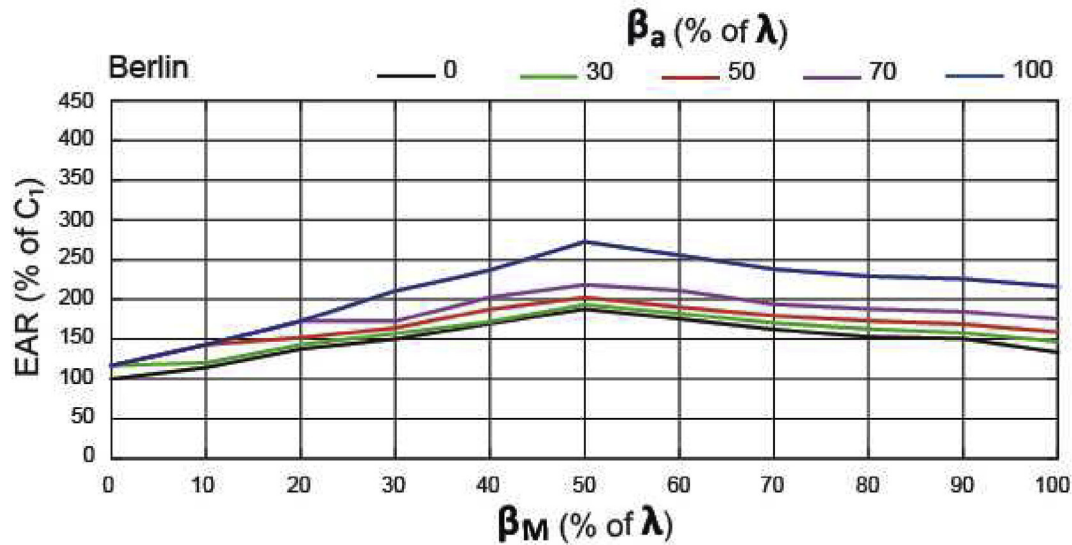


Fig. 16. Comparison EAR, in Berlin.

the SSLFR. Although Budapest receives 105.73% the direct horizontal irradiance of Berlin, the effect of latitude makes the EAR be greater at Berlin.

Figs. 13–17 shows the percentages, with respect to configuration C_1 , of the EAR, in Almeria, Rome, Budapest, Berlin and Helsinki, respectively. Notice in these figures that the positive effects of the longitudinal inclination of the mobile structure and the secondary reflector system on the EAR are greater at the locations with greater latitude.

4.3. Effects on the primary cost

Figs. 18–22 show the percentages, with respect to configuration C_1 , of the primary cost, in Almeria, Rome, Budapest, Berlin and Helsinki, respectively. As we see, modifying the longitudinal inclination of the mobile structure and the secondary reflector system with a low increase of the primary cost a high increase of the

energy is achieved.

By way of example, a comparison of the combination of β_M and β_a for which the greatest energy is obtained, is shown in Table 8. Another interesting comparison is for the combination of β_M and β_a providing the maximum EAR. These results are shown in Table 9.

5. Conclusions

In this study we analyze the effect of the longitudinal tilt angle of the rows of mirrors and the longitudinal tilt angle of the absorber tube on the performance of small-scale linear Fresnel reflectors at five European locations. Different combinations of β_M and β_a are analyzed and compared with the typical configuration of a large-scale linear Fresnel reflector.

We perform (to our knowledge, for the first time) the study of the effect of the inclination on three parameters: absorbed energy, energy-to-area ratio, and primary cost. We remark that in all

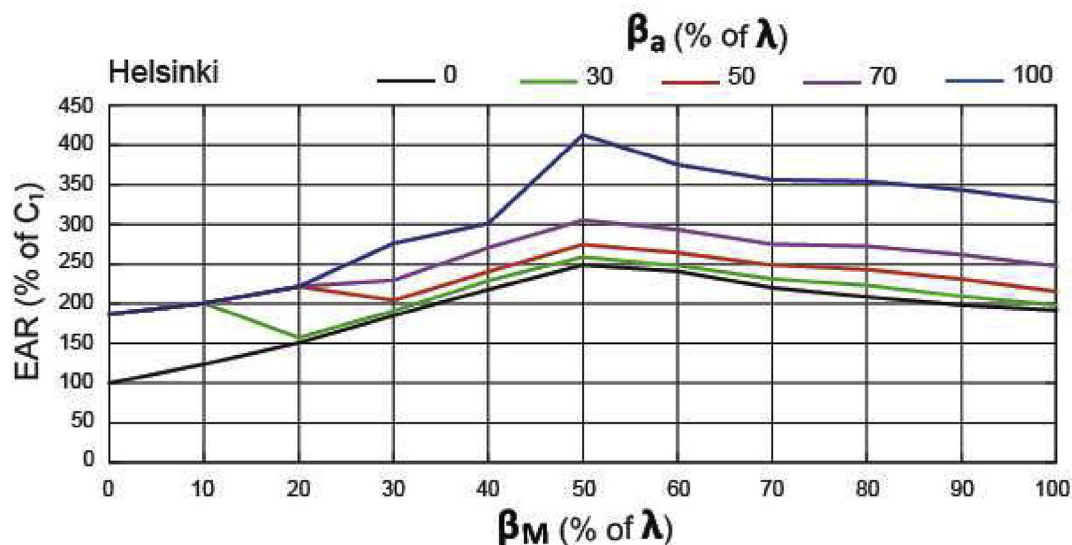


Fig. 17. Comparison EAR, in Helsinki.

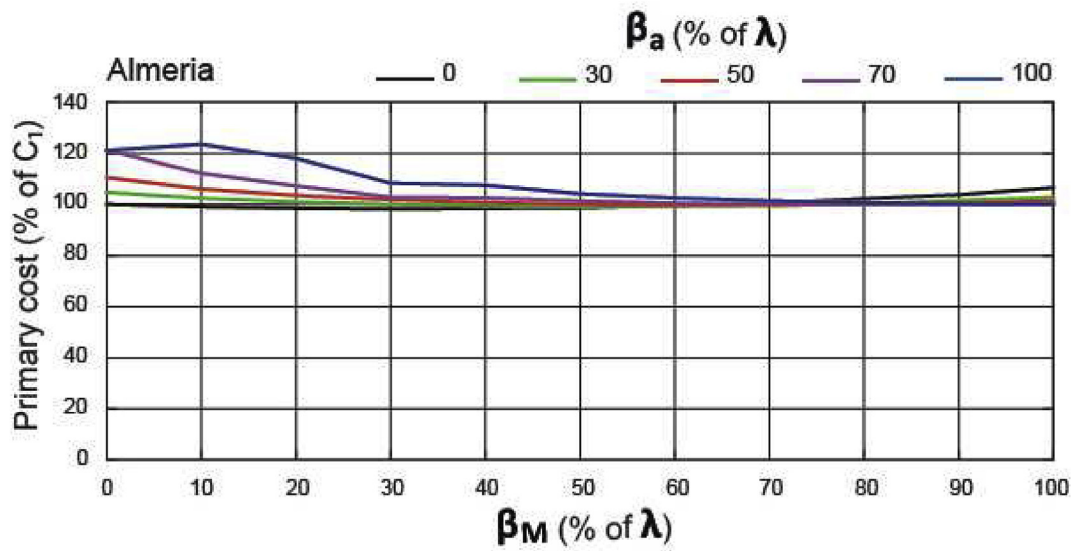


Fig. 18. Comparison primary cost, in Almeria.

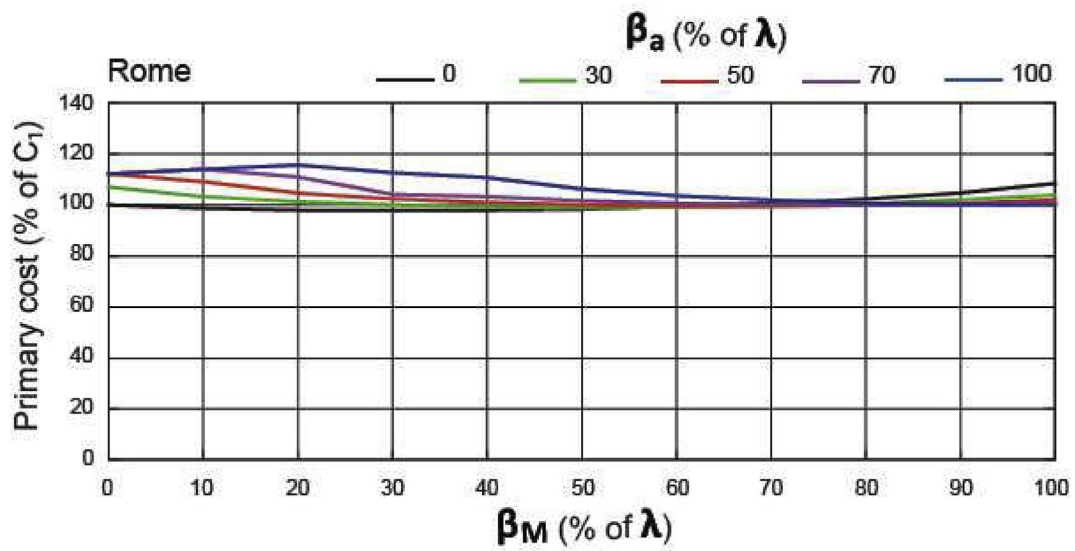


Fig. 19. Comparison primary cost, in Rome.

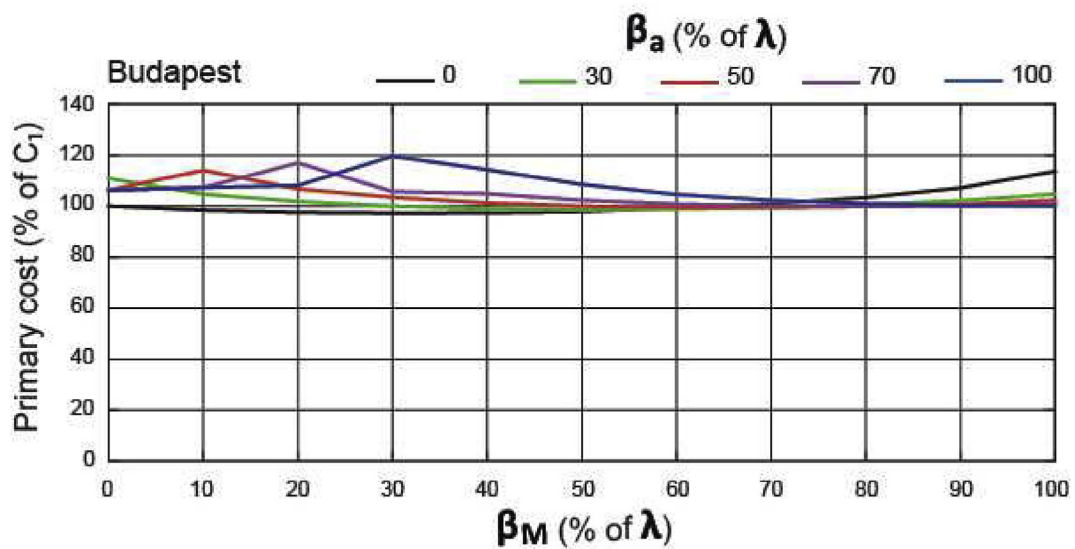


Fig. 20. Comparison primary cost, in Budapest.

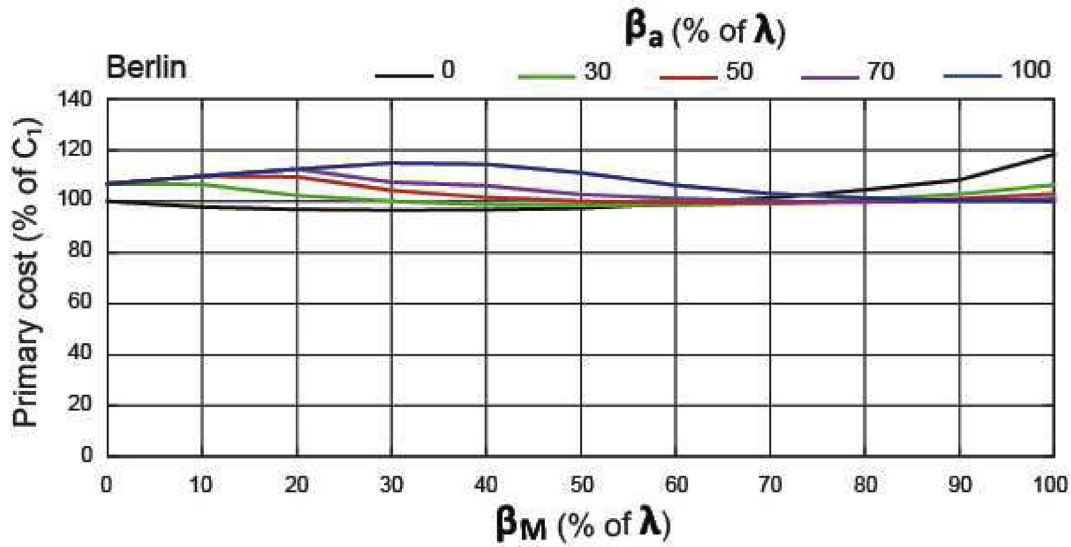


Fig. 21. Comparison primary cost, in Berlin.

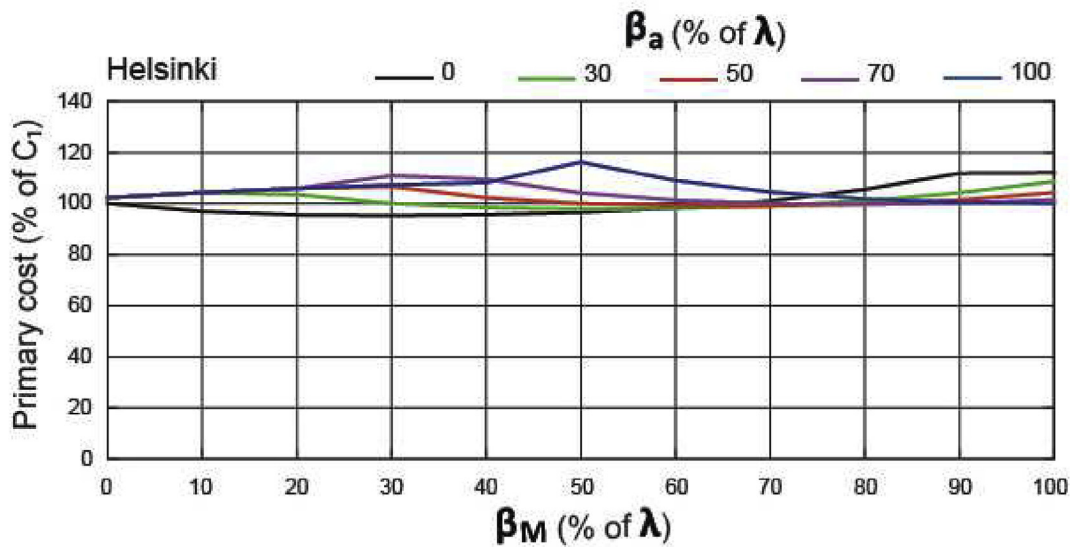


Fig. 22. Comparison primary cost, in Helsinki.

Table 8
Combination of β_M and β_a providing the maximum annual energy.

	β_M (% of λ)	β_a (% of λ)	Primary cost (% of C ₁)	E (% of C ₁)
Almeria	10	90	123.59	173.95
Rome	10	70	114.05	148.58
Budapest	20	70	116.97	156.11
Berlin	100	0	118.37	167.93
Helsinki	100	0	112.10	177.35

Table 9
Combination of β_M and β_a providing the maximum EAR.

	β_M (% of λ)	β_a (% of λ)	Primary cost (% of C ₁)	EAR (% of C ₁)
Almeria	50	100	104.18	142.54
Rome	50	100	106.27	179.60
Budapest	50	100	108.53	219.82
Berlin	50	100	111.18	272.30
Helsinki	50	100	116.24	412.76

climate areas the inclination provided by our method increases the absorbed energy and the energy-to-area ratio. Regarding the primary cost, we are able to evaluate the impact of the inclination on the cost and to relate the cost with the improvement in absorbed energy or energy-to-area ratio.

Another noticeable improvement with respect to the previous literature is the implications for urban applications of the SSLFR.

The area required for the SSLFR installation is an important aspect to be considered; therefore, we have divided the study into two possible scenarios: the available area is not a critical parameter (the energy absorbed by the absorber tube is evaluated), and the available area is a critical parameter (the energy-to-area ratio is evaluated). In both cases, the primary cost was evaluated and compared.

Next we summarize the main qualitative and quantitative conclusions of our study:

- An SSLFR with a longitudinal tilt angle of the rows of mirrors and a longitudinal tilt angle of the absorber tube shows good results in annual energy, and energy-to-area ratio.
- The combinations of β_M and β_a for which the maximum annual energy are obtained do not match those for which the EAR is maximum. The choice of either combination depends on the available surface.
- With a reduced increase of the primary cost one gets a high increase in the annual energy. The best results are obtained at the place with greatest latitude (Helsinki).
- When the secondary reflector system forms an angle of $\beta_a = 0^\circ$ with the horizontal plane and the mobile structure forms a specific angle with the horizontal plane, increasing β_M causes first a decrease in the energy absorbed by the absorber tube up to a minimum value and then an increase until $\beta_M = \lambda$.
- The combinations of β_M whose longitudinal tilt angle allow that the reflected rays by the mirrors in the longitudinal direction be always vertical at solar noon, throughout the year, reduce significantly the area required for SSLFR installation, showing improvements in the five cities.
- The best EAR outcome is obtained for the combination $\beta_M = \frac{\lambda}{2}$, $\beta_a = \lambda$. The greatest EAR value is obtained at Almeria, as it is the location receiving the most direct horizontal irradiance.

Acknowledgments

We wish to thank M. F. Fanjul, head of the CIFP-Mantenimiento y Servicios a la Producción vocational training school in La Felguera, Asturias, Spain, and the teacher F. Salguero for their work on the building of the prototype for the design presented in this paper.

References

- [1] T. Boermans, K. Bettgenhäuser, M. Offermann, S. Schimschar, Renovation tracks for Europe up to 2050: building renovation in Europe – what are the choices? *Ecofys* (2012) 1–52.
- [2] IEA, *Transition to Sustainable Buildings: Strategies and Opportunities to 2050*, International Energy Agency, 2013.
- [3] European Commission, *A Roadmap for Moving to a Competitive Low Carbon Economy in 2050*, 2011.
- [4] Directive 2012/27/EU, *On Energy Efficiency*, 2012.
- [5] M.S. Buker, S.B. Riffat, Building integrated solar thermal collectors – a review, *Renew. Sustain. Energy Rev.* 51 (2015) 327–346.
- [6] C. Tzivanidis, E. Bellos, The use of parabolic trough collectors for solar cooling – a case study for Athens climate, *Case Stud. Therm. Eng.* 8 (2016) 403–413.
- [7] B. Zou, J. Dong, Y. Yao, Y. Jiang, An experimental investigation on a small-sized parabolic trough solar collector for water heating in cold areas, *Appl. Energy* 163 (2016) 396–407.
- [8] T. Sultana, G.L. Morrison, G. Rosengarten, Thermal performance of a novel rooftop solar micro-concentrating collector, *Sol. Energy* 86 (2012) 1992–2000.
- [9] T. Sultana, G.L. Morrison, R.A. Taylor, G. Rosengarten, Numerical and experimental study of a solar micro concentrating collector, *Sol. Energy* 112 (2015) 20–29.
- [10] G. Mokhtar, B. Boussad, S. Noureddine, A linear Fresnel reflector as a solar system for heating water: theoretical and experimental study, *Case Stud. Therm. Eng.* Case 8 (2016) 176–186.
- [11] P. Bermejo, F.J. Pino, F. Rosa, Solar absorption cooling plant in Seville, *Sol. Energy* 84 (2010) 1503–1512.
- [12] F.J. Pino, R. Caro, F. Rosa, J. Guerra, Experimental validation of an optical and thermal model of a linear Fresnel collector system, *Appl. Therm. Eng.* 50 (2013) 1463–1471.
- [13] M.A. Serag-Eldin, Thermal design of a roof-mounted CLFR collection system for a desert absorption chiller, *Int. J. Sustain. Energy* 33 (2014) 506–524.
- [14] N. Velázquez, O. García-Valladares, D. Saucedo, R. Beltrán, Numerical simulation of a linear Fresnel reflector concentrator used as direct generator in a solar-GAX cycle, *Energy Convers. Manag.* 51 (2010) 434–445.
- [15] L. Zhou, X. Li, Y. Zhao, Y. Dai, Performance assessment of a single/double hybrid effect absorption cooling system driven by linear Fresnel solar collectors with latent thermal storage, *Sol. Energy* 151 (2017) 82–94.
- [16] A. Barbón, J.A. Sánchez-Rodríguez, L. Bayón, N. Barbón, Development of a fiber daylighting system based on a small-scale linear Fresnel reflector: theoretical elements, *Appl. Energy* 212 (2018) 733–745.
- [17] N. El Gharbia, H. Derball, S. Bouaichaoua, N. Said, A comparative study between parabolic trough collector and linear Fresnel reflector technologies, *Energy Procedia* 6 (2011) 565–572.
- [18] M.J. Montes, C. Rubbia, R. Abbas, J.M. Martínez-Val, A comparative analysis of configurations of linear Fresnel collectors for concentrating solar power, *Energy* 73 (2014) 192–203.
- [19] J.D. Nixon, P.A. Davies, Construction and experimental study of an elevation linear Fresnel reflector, *J. Sol. Energy Eng.* 138 (2016), 031001.
- [20] A. Barbón, N. Barbón, L. Bayón, J.A. Otero, Theoretical elements for the design of a small-scale linear Fresnel reflector: frontal and lateral views, *Sol. Energy* 132 (2016) 188–202.
- [21] A. Barbón, N. Barbón, L. Bayón, J.A. Otero, Optimization of the length and position of the absorber tube in small-scale Linear Fresnel concentrators, *Renew. Energy* 99 (2016) 986–995.
- [22] A. Barbón, N. Barbón, L. Bayón, J.A. Sánchez-Rodríguez, Parametric study of the small-scale linear Fresnel reflector, *Renew. Energy* 116 (2018) 64–74.
- [23] D. Pulido-Iparraquirre, L. Valenzuela, J.J. Serrano-Aguilera, A. Fernández-García, Optimized design of a Linear Fresnel reflector for solar process heat applications, *Renew. Energy* 131 (2019) 1089–1106.
- [24] G. Morin, J. Dersch, W. Platzer, M. Eck, A. Häberle, Comparison of linear Fresnel and parabolic trough collector power plants, *Sol. Energy* 86 (2012) 1–12.
- [25] Directive 2009/28/EC, *On the Promotion of the Use of Energy from Renewable Sources*, 2009.
- [26] European Commission, *A Policy Framework for Climate and Energy in the Period from 2020 to 2030*, 2014.
- [27] Directive 2018/30/EC, *On the Promotion of the Use of Energy from Renewable Sources*, 2018.
- [28] Odyssee-Mure, *Energy efficiency trends in buildings in the EU Lessons from the ODYSSEE MURE project*. <http://www.odyssee-mure.eu/publications/br/fresnel-efficiency-trends-policies-buildings.pdf>, 2015.
- [29] H. Bryan, H. Rallapalli, J. Jin Ho, Designing a solar ready roof: establishing the conditions for a high-performing solar installation, in: 39th ASES National Solar Conference, vol. 5, 2010, pp. 4081–4110.
- [30] L. Bergamasco, P. Asinari, Scalable methodology for the photovoltaic solar energy potential assessment based on available roof surface area: application to Piedmont Region (Italy), *Sol. Energy* 85 (2011) 1041–1055.
- [31] B. Fifth, P. Torcellini, N. Long, Assessment of the Technical Potential for Achieving Zero-Energy Commercial Buildings, *ACEEE Summer Study Pacific Grove*, 2006.
- [32] A. Barbón, J.A. Sánchez-Rodríguez, L. Bayón, C. Bayón-Cueli, Cost estimation relationships of a small scale linear Fresnel reflector, *Renew. Energy* 134 (2019) 1273–1284.
- [33] D.N. Korres, C. Tzivanidis, Development of two new semi-empirical formulas for estimation of solar absorptance in circular cavity receivers, *Therm. Sci. Eng. Prog.* 10 (2019) 147–153.
- [34] A. Barbón, L. Bayón, C. Bayón-Cueli, N. Barbón, A study of the effect of the longitudinal movement on the performance of small scale linear Fresnel reflectors, *Renew. Energy* 138 (2019) 128–138.
- [35] PVGIS. Joint Research Centre (JRC), 2019. Available on line at, http://re.jrc.ec.europa.eu/pvg_tools/en/tools.html#PVP.
- [36] Y. Zhu, J. Shi, Y. Li, L. Wang, Q. Huang, G. Xu, Design and thermal performances of a scalable linear Fresnel reflector solar system, *Energy Convers. Manag.* 146 (2017) 174–181.
- [37] Y. Zhu, J. Shi, Y. Li, L. Wang, Q. Huang, G. Xu, Design and experimental investigation of a stretched parabolic linear Fresnel reflector collecting system, *Energy Convers. Manag.* 126 (2016) 89–98.
- [40] J.A. Duffie, W.A. Beckman, *Solar Engineering of Thermal Processes*, fourth ed., John Wiley & Sons, New York, 2013.
- [41] V.M. Sharma, J.K. Nayak, S.B. Kedare, Effects of shading and blocking in linear Fresnel reflector field, *Sol. Energy* 113 (2015) 114–138.
- [42] P.H. Theunissen, W.A. Beckman, Solar transmittance characteristics of evacuated tubular collectors with diffuse back reflectors, *Sol. Energy* 35 (1985) 311–320.
- [43] European Commission, *Towards nearly zero-energy Buildings*. https://ec.europa.eu/energy/sites/ener/files/documents/nzeb_full_report.pdf. (Accessed 11 November 2018).